The EMBO Journal (2011) 30, 2881–2893 | © 2011 European Molecular Biology Organization | All Rights Reserved 0261-4189/11
www.embojournal.org

THE EMBO JOURNAL

Atomic force microscopy captures MutS tetramers initiating DNA mismatch repair

Yong Jiang[1,2,*] and Piotr E Marszalek[2,*]

[1]School of Chemistry and Chemical Engineering, Southeast University, Jiangsu, PR China and [2]Center for Biologically Inspired Materials and Material Systems, Department of Mechanical Engineering and Materials Science, Duke University, Durham, NC, USA

In spite of extensive research, the mechanism by which MutS initiates DNA mismatch repair (MMR) remains controversial. We use atomic force microscopy (AFM) to capture how MutS orchestrates the first step of *E. coli* MMR. AFM images captured two types of MutS/DNA complexes: single-site binding and loop binding. In most of the DNA loops imaged, two closely associated MutS dimers formed a tetrameric complex in which one of the MutS dimers was located at or near the mismatch. Surprisingly, in the presence of ATP, one MutS dimer remained at or near the mismatch site and the other, while maintaining contact with the first dimer, relocated on the DNA by reeling in DNA, thereby producing expanding DNA loops. Our results indicate that MutS tetramers composed of two non-equivalent MutS dimers drive *E. coli* MMR, and these new observations now reconcile the apparent contradictions of previous 'sliding' and 'bending/looping' models of interaction between mismatch and strand signal.

The EMBO Journal (2011) **30,** 2881–2893. doi:10.1038/emboj.2011.180; Published online 10 June 2011
Subject Categories: genome stability & dynamics
Keywords: atomic force microscopy; DNA loops; mismatch repair; MutS

Introduction

DNA mismatch repair (MMR) is a conserved pathway targeting mismatched base pairs that arise through DNA replication errors and during genetic recombination (Modrich, 1987; Modrich and Lahue, 1996; Kunkel and Erie, 2005; Iyer *et al*, 2006). In *E. coli*, the strand specificity necessary for removal of DNA biosynthetic errors from the daughter strand is based on the transient absence of d(GATC) methylation in newly synthesized DNA (Pukkila *et al*, 1983). Genetic and biochemical experiments have implicated 11 gene products in the methyl-directed reaction (Iyer *et al*, 2006) and repair in this system has been reconstituted using purified proteins (Lahue *et al*, 1989; Cooper *et al*, 1993; Burdett *et al*, 2001; Viswanathan *et al*, 2001). Repair is initiated by the binding of MutS to a mismatch or to a small insertion–deletion loop (Allen *et al*, 1997). Subsequently, ATP-, MutS-, and MutL-dependent activation of MutH endonuclease results in an incision of the unmethylated strand at a d(GATC) site that can reside at a distance of 1000 bp or more from the mismatch, producing a strand break either 3′ or 5′ to the mismatch. An excision system that includes DNA helicase II and an appropriate single-strand exonuclease is loaded at the strand break in a MutS- and MutL-dependent manner. Excision directed by a 3′-strand break depends on the 3′–5′ hydrolytic activity of exonuclease I, exonuclease VII, or exonuclease X, while the 5′–3′ activity of either RecJ exonuclease or exonuclease VII can support hydrolysis directed by a 5′-strand break. Following excision of the unmethylated strand to a point beyond the mismatch, the excised DNA segment is resynthesized and covalent continuity is restored to the repaired strand by the action of DNA ligase.

A key unanswered question with respect to MMR in *E. coli* is how MutS directs MutH to incise at a site, which can be separated by a considerable distance (1000 bp or more) from the mismatch. And after the incision, how the orientation-dependent loading of the excision system occurs? Three different models have been proposed to explain the interactions of the mismatch and incision sites. One postulates ATP-dependent diffusion (Gradia *et al*, 1999; Acharya *et al*, 2003) and hydrolysis-dependent unidirectional translocation (Allen *et al*, 1997; Blackwell *et al*, 2001b) of MutS or of a MutS/MutL complex along the helix contour between the mismatch and the strand signal. Another model suggests that mismatch recognition by MutS triggers polymerization of a second protein along the helix between the two DNA sites (Modrich, 1987; Hall *et al*, 2001). The third model proposes that the two sites interact by a DNA bending mechanism, with MutS remaining at or near the mismatch; this model does not require signalling along the helix contour. And a variant of this model includes the supposition that MutS bound to a mismatch site in trans can activate MutH (Junop *et al*, 2001; Schofield *et al*, 2001; Wang and Hays, 2004).

MutS-mediated loops in DNA have been observed by electron microscopy and atomic force microscopy (AFM; Allen *et al*, 1997; Jia *et al*, 2008); however, it is not clear whether the MutS oligomer involved in loop formation is a dimer, tetramer, or some other oligomeric structure. This point, namely, the oligomeric state of MutS in MMR, is another aspect of the MMR mechanism that remains controversial. The existence of tetramers of MutS has been demonstrated by analytical ultracentrifugation and inferred from gel electrophoresis assays (Bjornson *et al*, 2003; Mendillo *et al*, 2007). However, studies with MutS mutants defective in tetramer formation have yielded conflicting results, with some studies indicating severe defects in key MMR functions (Bjornson *et al*, 2003; Calmann *et al*, 2005;

*Corresponding authors. Y Jiang, School of Chemistry and Chemical Engineering, Southeast University, Chemistry Building, Dongnandaxue Road 2#, Jiangning, Nanjing, Jiangsu 211189, PR China.
Tel.: +86 139 139 931 09; Fax: +86 25 8379 3456;
E-mail: yj@seu.edu.cn or PE Marszalek, Center for Biologically Inspired Materials and Material Systems, Department of Mechanical Engineering and Materials Science, Duke University, 144 Hudson Hall, Durham, NC 27708, USA. Tel.: +1 919 660 5381; Fax: +1 919 660 8963;
E-mail: pemar@duke.edu

Received: 21 February 2011; accepted: 10 May 2011; published online: 10 June 2011

Manelyte *et al*, 2006; Huang and Crothers, 2008), while other researchers observed smaller MMR defects (Mendillo *et al*, 2007). Therefore, some researchers propose that MutS dimers have the key role in *E. coli* MMR (Mendillo *et al*, 2007), while others suggest that the functional unit is a tetramer (Huang and Crothers, 2008).

AFM allows direct imaging of DNA, proteins, and their complexes at the single molecule level (Hansma *et al*, 2004) and is ideal for visualizing various DNA transactions (Mikheikin *et al*, 2006; Shlyakhtenko *et al*, 2007). So far, however, AFM has only been rarely employed in the investigations of MMR, whose primary focus was on unravelling the mechanism by which MutS detects mismatches (Wang *et al*, 2003; Jia *et al*, 2008; Tessmer *et al*, 2008).

In this study, we rechecked the recognition mechanisms of MutS detecting mismatch in detail by AFM. We captured free MutS oligomeric assemblies and characterized their interactions with homoduplex and heteroduplex DNA molecules in the absence or presence of various nucleotides, as well as in the absence or presence of protein 'end blocks' or 'roadblocks'. Our results show that MutS binds to mismatched DNA in several configurations, including one that results in the formation of a DNA 'loop' with two closely associated MutS dimers at its base. DNA loops occurred 5–18 times more frequently on mismatch-containing DNA than on homoduplex DNA, and increased in size when incubated in the presence of ATP. Importantly, our results show that in the presence of ATP, one MutS dimer remained at or near the mismatch site, while the other relocated on the DNA while maintaining close contact with the first dimer. Our observations provide evidence for the previously hypothesized non-equivalence of two MutS dimers within the tetramer (Obmolova *et al*, 2000; Bjornson and Modrich, 2003; Natrajan *et al*, 2003). These findings provide new mechanistic insights into how the two critical MMR DNA sites interact. This interaction is likely mediated not by one but by two MutS dimers and a DNA looping mechanism in which one MutS dimer moves along the helix in an ATP enhanced process.

Results

We used volumetric analysis (Ratcliff and Erie, 2001; Horcas *et al*, 2007) of AFM images to determine the oligomeric states of free MutS at near-physiological ionic strength and MutS concentration. Figure 1A shows a typical AFM image of MutS on fresh mica in the absence of any nucleotide; Figure 1B is a treated image using the flooding method (Horcas *et al*, 2007) showing magnified oligomeric structures of MutS in the boxed area of Figure 1A. The distribution of the measured volumes of MutS complexes in a large number of images is shown in the distribution histogram in Figure 1C. At the same time, the inset figure in Figure 1C shows the distribution histogram of the MutS at same experimental condition except ATP was added as comparison. Fitting Gaussian distributions to three independent volume distribution data reveals that the measured MutS volumes fall into three independent distributions with peak values of 63 ± 16, 187 ± 37, and $414 \pm 57\,nm^3$ (mean ± s.d.).

By measuring AFM volumes of a set of reference proteins (see Supplementary Figure S1), we obtained a linear relationship between the measured volumes and their molecular weights (Ratcliff and Erie, 2001). Using this relationship as a standard, we determined the molecular weights of MutS complexes in images similar to those shown in Figure 1. The molecular weights determined by this method for the MutS complexes observed (92 ± 10, 165 ± 22, and 300 ± 34 kDa) correspond closely to the values of 95, 190, and 380 kDa expected for MutS monomer, dimer, and tetramer, respectively. This result strongly suggests that the MutS oligomeric assemblies represented by the three peak volume distributions observed in our AFM images are MutS monomers, dimers, and tetramers. These assemblies could also be clearly identified by visual inspection of AFM images of MutS (see spots labelled M as monomer, D as dimer, and T as tetramer in Figure 1B). MutS tetramers appeared in two different forms: one appeared as a simple association of two dimers (marked T1 in Figure 1B); the other resembled an amalgamation of two dimers into a larger particle (T2 in Figure 1B). These two apparent forms (T1 and T2) have similar volumes as measured by AFM (data not shown) and their different appearance could be a consequence of different orientations of tetramers on the mica surface.

The number of MutS molecules in each peak in the volume distribution was integrated, and the integrated values were multiplied by the degree of oligomerization to obtain the weight percentages of MutS in each of the oligomeric structures observed (Figure 1D). In the absence of nucleotide, $41 \pm 2\%$ of the MutS particles had volumes similar to that expected for a dimer; substantial amounts of monomer- and tetramer-sized MutS (28 ± 3 and $31 \pm 4\%$, respectively) were also seen in Figure 1D. The inclusion of all adenine nucleotides (ADP, ATP, AMPPnP, or a mixture of equal parts ADP and AMPPnP) in the incubation solution containing MutS decreased the amount of monomer observed from 28 to ~5% and increased the relative amounts of dimer and tetramer to ~53 and ~42% shown in Figure 1D. Although all nucleotides had a significant effect on the proportion of monomer present, there were only small differences in the proportions of monomer, dimer, and tetramer depending on which nucleotide was present.

Figure 2 shows histograms representing the percentage of MutS molecules found in each of the three oligomeric states after incubation of MutS with linear homoduplex or G-T heteroduplex DNA (41 or 201 bp in length). The presence of 41-bp DNA (homoduplex or G-T mismatch) either with or without added nucleotides had minimal effect on the distribution of MutS aggregation states (Figure 2A). However, inclusion of 201-bp DNA significantly increased the percentage of MutS appearing as tetramer, particularly in the presence of adenine nucleotide (Figure 2B). In the presence of both 201-bp DNA and 0.5 mM ADP, ATP, AMPPnP, or ADP + AMPPnP, the proportion of MutS existing as apparent tetramers increased from ~40% to ~70%. Thus, at a MutS concentration of 100 nM, close to its estimated *in vivo* concentration (Feng *et al*, 1996), tetramers were the main form observed for MutS bound to DNA. The results of the control experiments (data not shown) confirmed that, when the concentrations of MutS and 41-bp DNA or 201-bp DNA were changed, the change in the ratio of dimer to tetramer was minimal. This observation supports the conclusion that the percentages of MutS dimers and tetramers were not affected by the concentration of DNA, but rather by the length of the DNA.

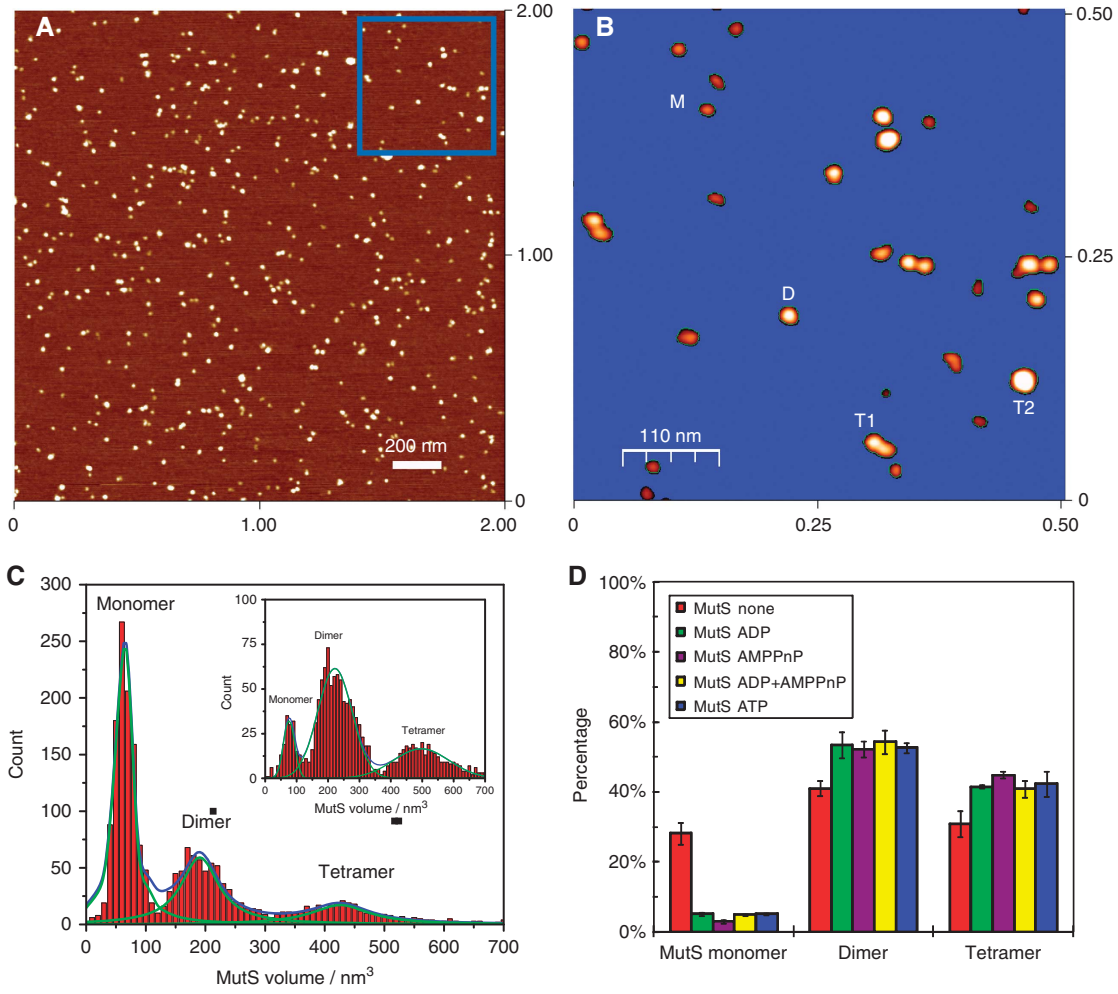

Figure 1 Volume analysis of MutS. MutS (100 nM) was incubated in the absence of a nucleotide in 20 mM Tris–HCl (pH 7.5), 100 mM K^+ glutamate, 5 mM $MgCl_2$, and 0.4 mM DTT for 10 min before deposition on mica, washing, and air-drying as described in Materials and methods. (**A**) A typical AFM image showing MutS on mica; the scan size of this image is $2 \times 2\,\mu m^2$. (**B**) An enlargement of the area shown in the blue box of image (**A**). The mica surface was flooded by a blue colour to make MutS more apparent. The size of this image is $0.5 \times 0.5\,\mu m^2$. Protein particles labelled 'M', 'D', and 'T' were identified as a MutS monomer, dimer, and tetramer, respectively, by further comparison with the volumes of proteins of known molecular weights (Supplementary Figure S1). (**C**) The histogram showing the volume distribution of MutS particles measured in images similar to those shown in (**A**). The inset figure shows the volume distribution of MutS particles in the presence of ATP for comparison. Three individual peaks were verified as monomer, dimer, and tetramer, respectively, according to their volumes. (**D**) Percentage histogram showing the percentage of MutS found in each oligomeric state in the presence of various nucleotides (0.5 mM). The bars, from left to right, indicate no nucleotide (red), ADP (green), AMPPnP (purple), half ADP and half AMPPnP (yellow), and ATP (blue). Error bars indicate ± s.d. The bar graphs are percentages of MutS monomer presented as each species.

In order to address the interaction of MutS with DNA in further detail, images were prepared after incubation of MutS with linear 1120-bp heteroduplex DNA containing a single G-T mismatch (for a detailed description of this DNA, see Supplementary Figure S2). Two types of MutS/DNA complex were observed in these experiments. The first involved MutS binding at a single location (single-site binding). MutS proteins involved in single-site binding might be dimers or tetramers (see Table I), and most were located close to the mismatch site. Figure 3A and C show examples of single-site binding of MutS in the absence of any nucleotide and in the presence of ATP, respectively, to a G-T mismatch-containing DNA with two biotinylated ends which had been previously bound with monofunctional streptavidin (Howarth *et al*, 2006) before incubation with MutS. Experiments were also performed using single-end-biotinylated DNA that had been previously bound with streptavidin, and with DNA that had not been incubated with streptavidin. Supplementary Figure S3 shows a detailed analysis of the distribution of single-site-bound MutS on streptavidin-bound biotinylated DNAs. Single-site-bound MutS can be divided into two groups: specific bound and non-specific bound. The specific-bound MutS located at the relative position of 50 ± 6 and 50 ± 5% of the relative DNA length before and after ATP was added (Supplementary Figure S3C and D).

The second type of MutS/DNA complex that was observed frequently promoted a segment of DNA to form a loop, at the base of which were situated two closely associated MutS dimers or a MutS tetramer. Figure 3B illustrates MutS/DNA loop binding in the absence of nucleotide. Under these conditions, loops formed most frequently by two easily distinguishable, closely associated MutS dimers. When ATP was present, loop formation was most often mediated by a MutS tetramer that covered the DNA strands at the base of the loop (Figure 3D).

The oligomeric forms of MutS bound to 1120-bp DNA in single-site and loop binding were verified by AFM volume measurement (Table I). In the absence of ATP, the statistical distribution of the volumes of single-site-bound MutS yielded two peaks, one corresponding closely to the expected molecular weight of a MutS dimer (181 ± 27 kDa) and the other to the expected molecular weight of a MutS tetramer (361 ± 29 kDa). The calculated molecular weight of loop-bound MutS almost always corresponded to that of a tetramer (365 ± 42 kDa). In the presence of ATP, MutS dimers and tetramers appeared larger than in its absence (Table I). Single-site-bound MutS exhibited an apparent increase of 28–45% in volume, while free MutS appeared 17–20% larger (Table I). Furthermore, while in the absence of ATP loops appeared to contain two associated MutS dimers, the outline of each of which was separately distinguishable (example shown in Figure 3B), in the presence of ATP the two MutS dimers at the base of loops appeared to merge into a more unified structure (Figure 3D), with an average volume ~28% larger than that of the loop-bound tetramers seen in the absence of ATP. These phenomena may indicate a conformational change in MutS that depends on the presence of both ATP and DNA.

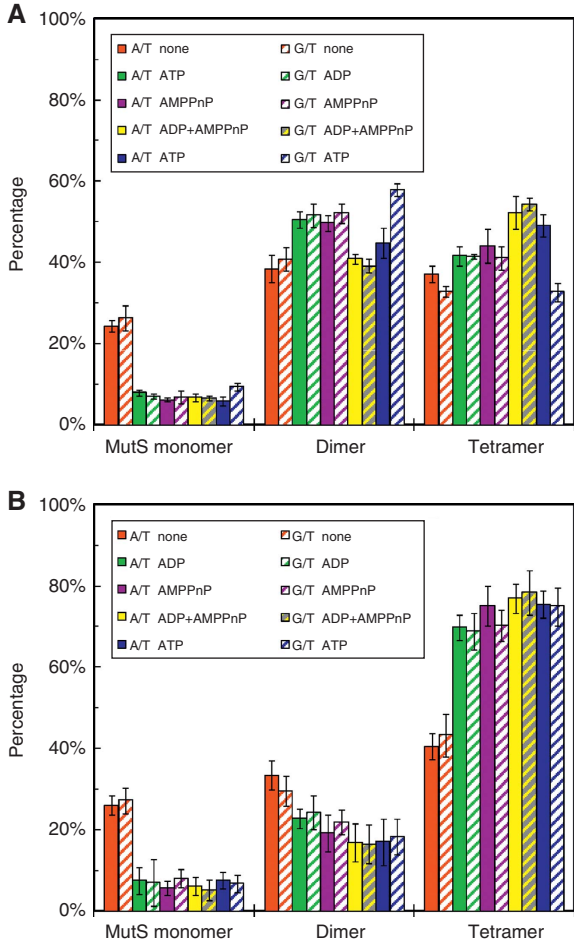

Figure 2 Distribution of MutS monomers, dimers, and tetramers in the presence of DNA oligomers and various nucleotides. MutS (100 nM) was incubated for 5 min in 20 mM Tris–HCl (pH 7.5), 100 mM K^+ glutamate, 5 mM $MgCl_2$, and 0.4 mM DTT plus 0.5 mM of the indicated nucleotide and either 200 nM 41-bp homoduplex DNA (panel (**A**), A-T), 200 nM 41-bp heteroduplex DNA (panel (**A**), G-T), 200 nM 201-bp homoduplex DNA (panel (**B**), A-T), or 200 nM 201-bp heteroduplex DNA (panel (**B**), G-T) followed by deposition on mica and imaging. Error bars indicate ± s.d. The bar graphs are percentages of MutS monomers as each species.

In order to determine the effect of ATP on loop size, we incubated MutS with 1120-bp G-T DNA for 10 min in the absence and presence of ATP (Figures 3 and 4). We then measured the resulting contour lengths of the DNA segments representing the 'short leg', 'loop contour', and 'long leg' of the DNA. Supplementary Figure S2F–G provides details of how the length of loop contour, short leg, and long leg were defined and measured. Figure 4A and E show the relative length distribution of the short legs, loop contours, and long legs of double-end-biotinylated DNA previously bound with streptavidin after incubation with MutS for 10 min in the absence or presence of ATP. The lengths of short legs, loop contours, and long legs were measured and fitted with Gaussian distributions (Figure 4B–D and F–H). In the absence of ATP, the lengths of the long legs fall into a Gaussian distribution centered at 46 ± 5% of the DNA length (Figure 4D). When ATP was included, the lengths of long leg remained centered at 47 ± 9% but the distribution broadened (Figure 4H). A comparison of Figure 4D and H shows that in the absence of nucleotide, the standard deviation is 5, while in the presence of ATP, the standard deviation increased to 9. However, the most important finding is that the mean of the Gaussian distribution of the loop contour length increased by about 15% (22 ± 5% for no nucleotide in Figure 4C and 37 ± 11% for adding ATP in Figure 4G) of the total DNA

Table I Volumes of MutS as measured from AFM images prepared in the absence or presence of DNA and ATP

Volume measurements of MutS	Free MutS dimer	Free MutS tetramer	Single-site-bound MutS dimer	Single-site-bound MutS tetramer	Loop-bound MutS tetramer
w/o ATP					
Volume, nm^3	187 ± 37 (N = 640)	414 ± 57 (N = 355)	213 ± 45 (N = 13)	517 ± 50 (N = 11)	524 ± 71 (N = 12)
MW, kDa	165 ± 22	300 ± 34	181 ± 27	361 ± 29	365 ± 42
w/ATP					
Volume, nm^3	222 ± 55 (N = 820)	497 ± 89 (N = 400)	309 ± 49* (N = 12)	663 ± 109 (N = 19)	672 ± 93 (N = 13)
MW, kDa	186 ± 32	349 ± 52	238 ± 29	448 ± 64	453 ± 55
P-value volume	<0.0001	<0.0001	0.000074	0.00049	0.00034

Values represent mean ± s.d.; N indicates the number of proteins measured; P-values were obtained using Student's t-test. *This type of MutS is rare. For a free MutS sample, MutS (100 nM) was incubated in a buffer containing 20 mM Tris–HCl (pH 7.5), 100 mM K^+ glutamate, 5 mM $MgCl_2$, and 0.4 mM DTT for 5 min before deposition on mica, and the washing and air-drying was as described in Materials and methods. For MutS bound on DNA, MutS (50 nM) was incubated with 1120-bp G-T heteroduplex DNA (10 nM) in buffer containing 20 mM Tris–HCl (pH 7.5), 100 mM K^+ glutamate, 5 mM $MgCl_2$, 0.4 mM DTT with or without 0.5 mM ATP for 5 min. The average volumes of MutS images in AFM and the corresponding molecular weights shown in the table were determined as described in the text and in Materials and methods.

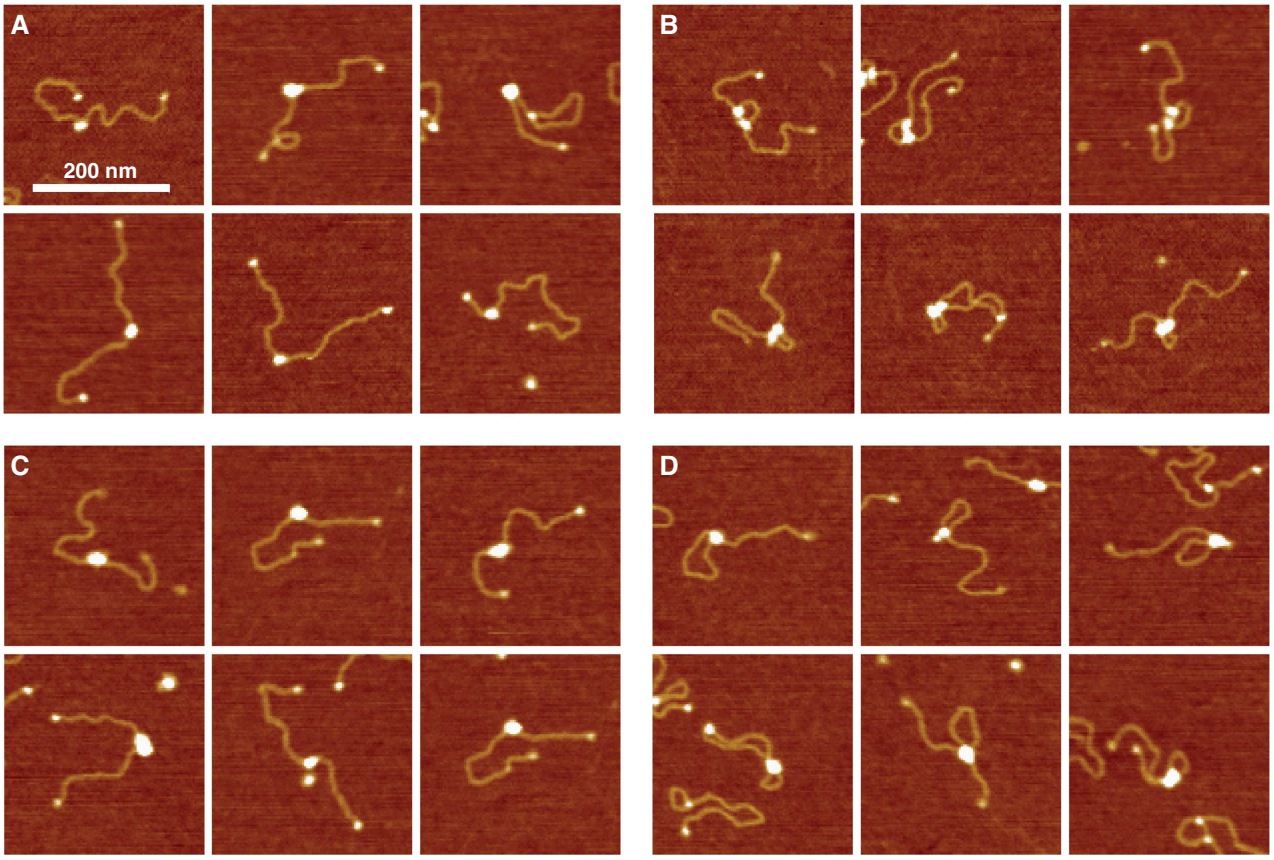

Figure 3 AFM images showing single-site binding and loop binding of MutS to heteroduplex DNA. (**A**, **B**) Images of MutS deposited in the absence of nucleotide. Images in (**A**) show MutS single-site binding on DNA; those in (**B**) show MutS loop binding. (**C**, **D**) Images of MutS deposited in the presence of 0.5 mM ATP. Images in (**C**) shows MutS single-site binding on DNA, while (**D**) shows loop binding. In both cases, the ends of DNA were previously bound with streptavidin. The scale bar indicates 200 nm.

length. And consequently, the length of short leg decreased from 32 ± 4% (Figure 4B) to 18 ± 7% (Figure 4F).

Because the end of the long leg remained at almost the same position (47–53%) in the presence or absence of ATP, the MutS dimer associated with the long leg remained at the mismatch site. However, when ATP was added, the length of the short leg became shorter and the size of the DNA loop increased.

A series of experiments were performed in which biotinylated DNA that was previously bound with streptavidin was incubated with MutS in the presence of various nucleotides. The lengths of the short legs, loop contours, and long legs of the resulting loops were measured and compared, by fitting a Gaussian distribution to histograms representing the distribution of the percentage of the DNA length represented by each segment. The results of these experiments (Table II) show that time, temperature, and specific nucleotide all affect the growth of the loops. When MutS and DNA were incubated in the presence of 0.5 mM ADP, average loop size was slightly smaller than that in the absence of nucleotide, and the loops were somewhat more homogeneous in size. Loop size after adding AMPPnP for 10 min was bigger (average increase 107 bp) than the loop generated at 'no nucleotide' condition and was similar to the loop size after incubation with ATP. Loops that formed on homoduplex DNA showed a bigger size and broader distribution than loops on G-T mismatch substrates.

For DNA that contained biotin at both ends, it is impossible to identify one end of the DNA from another. The mismatch position could be either 47 or 53% of the DNA length from the end in the looped complexes. Because of this uncertainty, the distribution for specific bindings that we determined was relatively broad. In order to eliminate this uncertainty, experiments were also performed using single-end-biotinylated DNA that had been previously bound with monovalent streptavidin on the single end. In this experiment, the mismatch position can be easily identified; it is located 53% of the DNA length from its streptavidin-labelled end. Supplementary Figure S2B provides detailed structure of this DNA.

The results are shown in Figures 5 (no ATP) and 6 (with ATP). Importantly, the DNA loops originated at or very close to the position of the mismatch. Some loops were formed between the mismatch and the biotinylated end while some were formed between the mismatch and the free DNA end. We analysed these cases separately (Figure 5A). For DNA molecules carrying the loops between the mismatch and the free DNA end (lower part of Figure 5A), the lengths of the long legs fall into a narrow Gaussian distribution centered exactly at 53 ± 3% of the DNA length (Figure 5D) coinciding with the location of the mismatch. For DNA molecules carrying a loop between the mismatch and the biotinylated end (upper part of Figure 5A), the length of the long legs is 46 ± 5% (Figure 5G) again, consistent with the location of

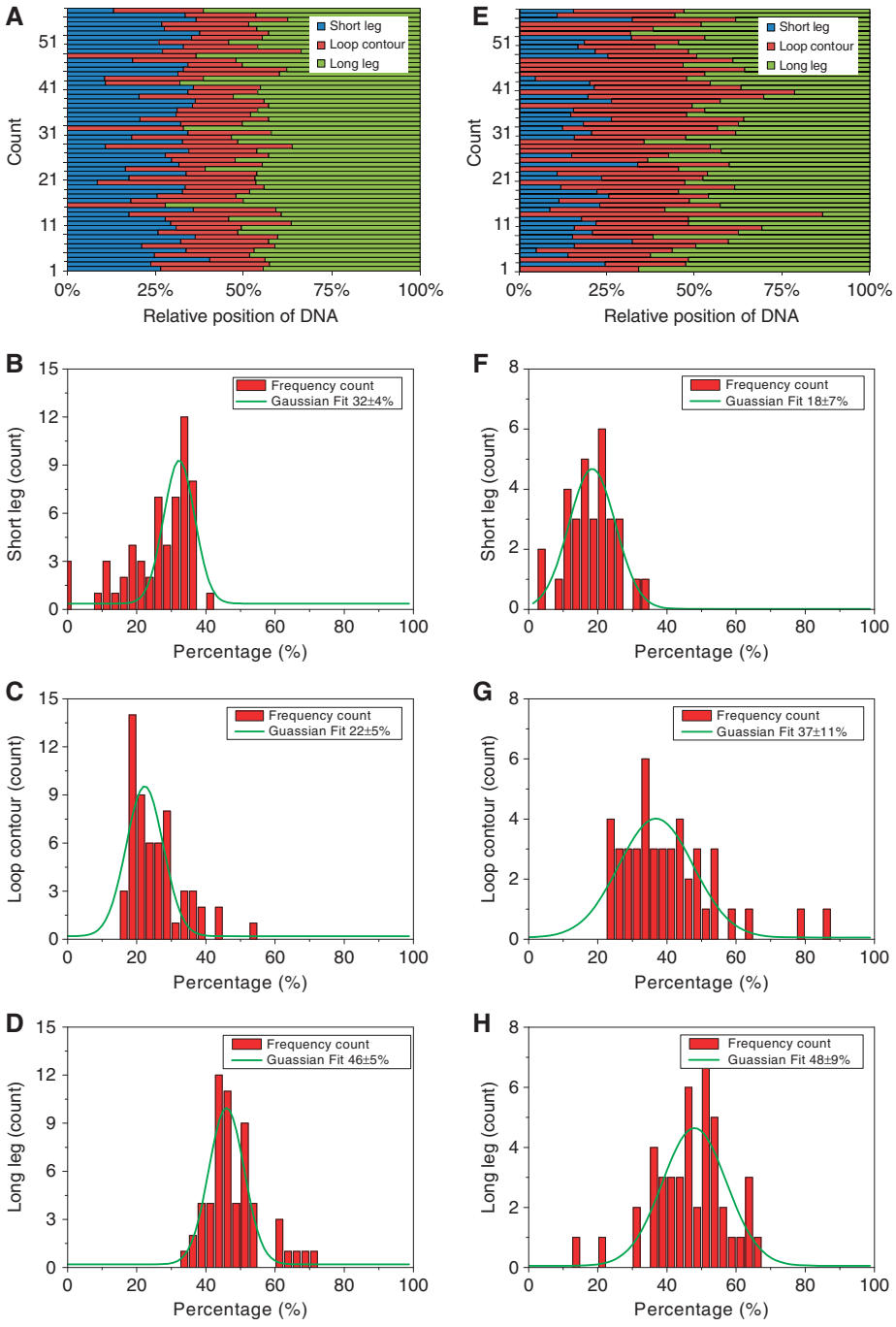

Figure 4 Normalized length distributions and Gaussian fits for MutS bound in loop configuration to heteroduplex DNA containing biotin at both DNA ends. MutS (100 nM) and 1120-bp G-T mismatch DNA (20 nM) that contained biotin at both ends and that had been previously bound with monovalent streptavidin (see Materials and methods) were incubated in 20 mM Tris–HCl (pH 7.5), 100 mM K^+ glutamate, 5 mM $MgCl_2$, and 0.4 mM DTT for 10 min at room temperature in the absence (**A**–**D**) or presence (**E**–**H**) of 0.5 mM ATP. Panels (**A**) and (**E**) show the contour lengths of each segment on individual DNA molecules. In each diagram, the left (blue) bar indicates the contour length of the shortest segment of DNA between MutS and the end of the DNA, the middle bar (red) indicates the contour length of the loop, and the right bar (green) indicates the contour length of the DNA segment between MutS and the other DNA end. The length of each segment was normalized to the total DNA length. The histograms below (**B**–**D**) and (**F**–**H**) show Gaussian fits of the contour length data. In the presence of ATP, the peak of the Gaussian distribution of the lengths of the short legs (the distance from the base of the loop to the nearest DNA end) decreased from 32 to 17% of the DNA length and the peak of the Gaussian distribution of the loop length increased from 22 to 36% of the DNA length, while the peak of the Gaussian distribution of the lengths of the long legs (the distance from the base of the loop to the furthest DNA end) remained at 46–47% of the DNA length.

the mismatch. When ATP was included, as shown in Figure 6, the distribution of the long leg lengths broadened but remained centered at 54 ± 5% (Figure 6D) and 48 ± 8% (Figure 6G) of the DNA length. At the same time the mean of the loop contour length increased by additional 20% of the DNA length when the loops formed between the mismatch and the free DNA end (Figure 6C) and by additional 13% of the DNA length (Figure 6F) when the loops formed on the

Table II Relative lengths of looped DNA molecules after incubation with MutS under different conditions

DNA/incubation conditions	Position/%		
	Short leg	Loop	Long Leg
G-T, no nucleotide, 10 min	32 ± 4	22 ± 5	46 ± 5
G-T, 0.5 mM ATP, 10 min	18 ± 7	37 ± 11	48 ± 9
G-T, 0.5 mM ATP, 10 sec	21 ± 9	31 ± 8	47 ± 9
G-T, 0.5 mM ATP, 10 sec on ice	21 ± 9	26 ± 6	50 ± 7
G-T, 0.5 mM ADP, 10 min	34 ± 3	19 ± 3	47 ± 4
G-T, 0.5 mM AMPPNP, 10 min	20 ± 13	32 ± 13	47 ± 10
Homoduplex, no nucleotide, 10 min	17 ± 10	40 ± 15	51 ± 16
G-T, no nucleotide, *Eco*RI bound, 10 min	27 ± 9	23 ± 3	47 ± 9
G-T, 0.5 mM ATP, *Eco*RI bound, 10 min	16 ± 4	31 ± 9	50 ± 12

Values represent mean ± s.d.
MutS (100 nM) and 1120-bp G-T mismatch/homoduplex DNA (20 nM) that contained biotin at both ends and had been previously bound with monovalent streptavidin were incubated in 20 mM Tris–HCl (pH 7.5), 100 mM K^+glutamate, 5 mM $MgCl_2$, and 0.4 mM DTT in the absence or presence of different nucleotides. All incubations were at room temperature (23°C) unless otherwise indicated. At the times shown, samples were deposited on APS-mica and the percentage of the DNA length corresponding to the short leg, long leg, and loop was determined from AFM images. For each experimental condition, about 50–60 DNAs with loops formed on them were analysed to determine length distributions. The data represent the mean values ± s.d. of the Gaussian distributions of the lengths of the short leg, loop contour, and long leg.

other side of the mismatch. A detailed analysis of the distribution of single-site-bound MutS on single-end-biotinylated DNAs previously bound with streptavidin is shown in Supplementary Figure S4. These results show that the MutS molecules that bound on one end of the loops remained on the mismatch whether or not ATP was present. When ATP was present, the short leg became shorter and the DNA loop size increased, consistent with the results obtained on double-end-biotinylated DNA (Figure 4). Furthermore, we observed that DNA loops can form and grow on both sides of the mismatch, which suggests that there is no preferred direction for MutS tetramers to produce and expand loops.

To determine whether internal roadblocks on the DNA could prevent the increases in loop size, we used DNA previously bound with $EcoRI_{E111Q}$. In the absence of ATP, the distribution of MutS showed no big difference whether or not *Eco*RI was added (Supplementary Figure S5). Also, the average size of loops formed in the presence of *Eco*RI and ATP was considerably larger than that measured in samples incubated with *Eco*RI and with ADP or with *Eco*RI but with no added nucleotide (Supplementary Figure S6; Table II). However, the loops formed in the presence of $EcoRI_{E111Q}$ blocks on MutS-bound DNA during the application of ATP for 10 min were on average smaller as compared with the loops formed on DNA under the same conditions but without $EcoRI_{E111Q}$ (a decrease from 37 to 31%; Table II; Supplementary Figure S6). This result suggests that the binding of $EcoRI_{E111Q}$ protein on DNA does prevent the increase in loop size. On DNA previously bound with $EcoRI_{E111Q}$ and subsequently incubated with MutS and ATP, loops which contained a protein (most likely $EcoRI_{E111Q}$) within the loop contour were sometimes seen, but loops with proteins only at the loop base and no visible proteins within the loop contour were much more frequent (74%) (Figure 7).

The dissociation constant (K_D) and the occupancy of DNA by MutS under different conditions were determined from AFM images and the data are presented in Supplementary Figure S7 and Supplementary Table S1. Our results are consistent with previous reports (Yang *et al*, 2005; Huang and Crothers, 2008), when one considers various lengths of DNA substrates used in various studies.

Discussion

MutS oligomeric states have been studied by means of ultracentrifugation, velocity sedimentation, and gel filtration. Previous studies have shown that MutS undergoes dimer-to-tetramer assembly, though the association constants for MutS dimers to tetramers are inconsistent (Bjornson *et al*, 2003; Lamers *et al*, 2004). In our current work, we evaluated the MutS dimer-to-tetramer conversion in the concentration range of 40–200 nM. Our results show that after deposition on mica from a solution containing 100 nM MutS (as monomer) in a buffer of comparable ionic strength to intracellular conditions (Feng *et al*, 1996), five-fold lower than the estimated *in vivo* MutS concentration (500 nM) in exponentially growing *E. coli* cells, approximately equal proportions of MutS exist in dimer and tetramer forms.

In the absence of any nucleotide, ~30% of the MutS monomers was identified, and the percentage dropped significantly to ~5% in the presence of all the nucleotides used. This result supports earlier observations about nucleotides' role in MutS dimerization (Lamers *et al*, 2004). The association constant for the dimer-to-tetramer transition is about $1.3 \times 10^7\,M^{-1}$, which is close to the value ($2.1 \times 10^7\,M^{-1}$) obtained by previous biochemical studies (Bjornson *et al*, 2003).

The addition of the adenosine nucleotide at concentrations expected to saturate both high-affinity (ATP or ADP) and low-affinity (ATP or ADP) binding sites on the two monomers within a dimer of MutS (Bjornson and Modrich, 2003), or of a mixture of the two nucleotides at saturating concentration, did not significantly alter the relative proportions of dimer and tetramer observed. When 201-bp DNA in length was included in the incubation, tetramer was the main form of MutS observed, and when both nucleotide and 201-bp DNA were present, the equilibrium was markedly shifted in favour of tetramers. Based on the AFM measurement alone, we do not know how much of the MutS was bound to DNA because the 41- and 201-bp DNA are too small to be imaged by AFM if they are bound to MutS. But based on the concentrations of both MutS and DNA used in our experiments (100 nM of MutS as monomer and 200 nM of DNA) and the known K_D of MutS/DNA complexes (21 nM) (Blackwell *et al*, 2001a), we can estimate that at this condition, >90% of MutS (93.8%) was occupied by DNA. These results suggest that the interaction of MutS with 201-bp DNA promotes the formation of tetramers, and that tetramer formation of MutS in complex with DNA is influenced by the interaction of MutS with adenosine nucleotides. The reason that the association constant for the dimer-to-tetramer transition did not change after 41-bp DNA was included might be that 41-bp DNA is too short to support binding of two MutS dimers side-by-side. However, the 201-bp DNA (both homoduplex and G-T mismatched) is long enough to accommodate and stabilize two dimers forming a tetramer structure. The similar

effect of homoduplex and G-T DNA on the dimer-to-tetramer transition suggests that MutS may scan DNA for mismatches as a tetramer. However, mechanistic details of the tetramerization step in the presence of DNA are presently missing and warrant further studies.

We observed MutS tetramers bound to DNA in a configuration in which one of the MutS dimers forming the tetramer appeared to be closely associated with the mismatch site, while the other occupied a non-specific site. In the absence of any nucleotides, the loops are quite small and contain

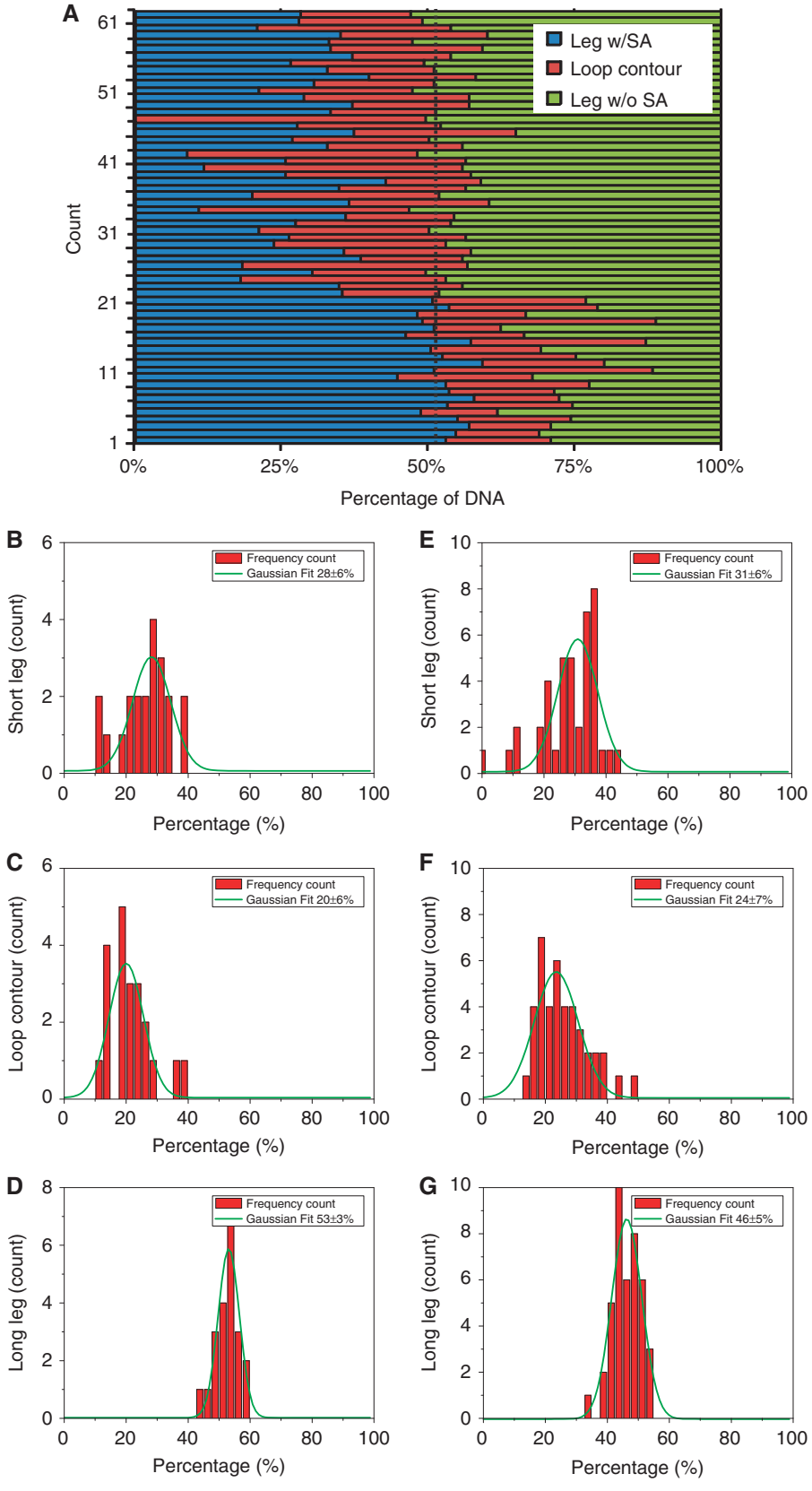

~250 bp of DNA. The DNA seems to have propensity to bend in this region, and this may promote loop formation for MutS interacting with DNA at two sites, mismatch and a non-specific site, or even two non-specific sites. Future projects will test whether a different DNA sequence with a lesser propensity for DNA bending may affect the frequency at which loops are formed. MutS molecules in this configuration were positioned at the base of DNA loops, the size of which increased in the presence of ATP. We also saw apparent MutS tetramers that appeared to associate with only a single site on the DNA. We most frequently observed loops on DNAs that had two biotinylated ends and that had been incubated with both streptavidin and $EcoRI_{E111Q}$ before incubation with MutS. The MutS occupancy of DNAs which were end blocked or which were additionally blocked by $EcoRI_{E111Q}$ at sites flanking the mismatch was about 2- to 3-fold higher than that of DNA that have not been blocked by any proteins in the presence of ATP; this suggests that MutS was 'trapped' on these DNAs by the presence of the protein blocks.

Initial attempts to evaluate ATP effects on MutS–DNA interaction were based in part on visualization of complexes of the *E. coli* protein with 6.4-kbp heteroduplex and homoduplex DNAs by electron microscopy (Allen *et al*, 1997). These experiments demonstrated the mismatch- and ATP-dependent formation of α-shaped DNA loop structures up to several kbp in size, in which MutS were bound at the base. Loop size was found to increase with time, and in the majority of molecules, the mismatch was present in the loop. There are a number of differences between the loops observed in the present study and those observed by Allen *et al*. In the latter, formation of loops depended on the presence of ATP, while the loops we observed occurred in the absence of nucleotides as well as in the presence of ADP, ATP, and AMPPnP. The loops we observed were actually less frequent when ATP or an ATP analogue was included in the incubation than when no nucleotide or ADP was added; depending on the conditions, loops were up to 50% more frequent in the absence of ATP than in its presence. The only exception to the difference in the frequency of loop formation was where DNAs had been previously incubated with both streptavidin and $EcoRI_{E111Q}$ before binding to MutS. Second, complexes between MutS and homoduplex DNA were observed very infrequently by Allen *et al* (1997) and both loop binding and 'no loop' binding largely depended on the presence of a mismatch. In our study, loops were also seen on homoduplex DNA ($2.4 \pm 0.3\%$) with a specificity about 18.1 times less than that on heteroduplex DNA under the same conditions (Supplementary data; Supplementary Table S1).

In addition, the size of the loops on homoduplex DNA ($40 \pm 15\%$) was much bigger than that on heteroduplex DNA ($22 \pm 5\%$), and at the same time their size distribution was also three times broader as compared with the loops formed on heteroduplex DNA (Table II). Our interpretation of this result is that in the absence of a mismatch, neither of MutS dimers that participated in the loop formation had to remain near the center of homoduplex DNA. In the present study, the size of the loops increased when either ATP or the non-hydrolysable ATP analogue AMPPnP was present, while in the study of Allen *et al*, non-hydrolysable ATP analogues failed to support large loop formation and ongoing loop growth was suppressed upon their addition to ATP-containing reactions. Another important difference between our results and those by Allen *et al* is that the DNA loops captured by AFM were on average significantly smaller than the loops captured by EM, which may be related to the smaller DNA substrate used in our study (1.12 versus 6.4 kbp).

Using AFM, Jia *et al* (2008) also reported similar α-shaped loops formed by MutS. The loops they imaged were independent of whether or not a mismatch was present in the DNA substrate. Furthermore, they found MutS D835R (tetramer deficient) and R194A/R198A/R275A mutants of MutS formed α-loops at a similar frequency as the wild-type MutS, suggesting that tetramer formation is not necessary for the formation of the loops in their system. However, that study did not provide evidence (e.g. by MutS volume measurements) that the MutS that formed α-loops was in a dimer configuration.

Using fast-scanning AFM, Crampton *et al* (2007) visualized translocation and extruded looping by *Eco*P15I restriction enzyme, which is similar to MutS displays anomalously low rates of ATP hydrolysis. In order to efficiently cleave DNA, *Eco*P15I requires two recognition sites separated by up to 3.5 kbp. They observed that DNA loops were formed by contact between specific site-bound *Eco*P15I and a non-specific region of DNA. Further they showed that *Eco*P15I translocation must also occur because when it is blocked by a Lac repressor protein, DNA cleavage is inhibited. This observation provides a plausible mechanism by which an enzyme could communicate rapidly between two non-contiguous DNA sites through a combination of translocation-coupled and DNA looping mechanism.

Our data show that in the absence of ATP, both end binding by streptavidin and roadblocking by *Eco*RI had no effect on binding and looping. But in the presence of ATP, binding by streptavidin and *Eco*RI increased the binding affinity and the fraction of loop binding (Supplementary data). On DNA previously bound with $EcoRI_{E111Q}$ and subsequently incubated with MutS and ATP, 74% of loops was seen which did not contain $EcoRI_{E111Q}$ within the loop contour. These loops were on average smaller than those loops formed in the presence of ATP on DNA without $EcoRI_{E111Q}$. Therefore, roadblocking by *Eco*RI seems to prevent the increase in loop size. Considering the residency half-life of $EcoRI_{E111Q}$ at a d(GAATTC) sequence is <40 min (Pluciennik and Modrich, 2007), one cannot exclude that part of *Eco*RI

Figure 5 Normalized length distributions for MutS bound in loop configuration to heteroduplex DNA containing biotin at a single DNA end in the absence of ATP. MutS (100 nM) and 1120-bp G-T mismatch DNA (20 nM) that contained biotin at the end further from the mismatch site and that had been previously bound with monovalent streptavidin (see Materials and methods) were incubated in 20 mM Tris–HCl (pH 7.5), 100 mM K^+ glutamate, 5 mM $MgCl_2$, and 0.4 mM DTT for 10 min at room temperature in the absence of ATP. Panel (**A**) shows the contour lengths of each segment on individual DNA molecules. The segment of DNA between MutS and the biotinylated end of the DNA is represented in blue, the loop is represented in red, and the segment of DNA between MutS and the other DNA end is represented in green. The position of the mismatch is indicated by a vertical dashed line. Two sets of loops can be observed from panel (**A**). Set one: the loops are between MutS and biotinylated ends, and set two: the loops are between MutS and free ends. The histograms (**B–D**) and (**E–G**) show Gaussian fits of the contour length data of these two sets of loops, respectively.

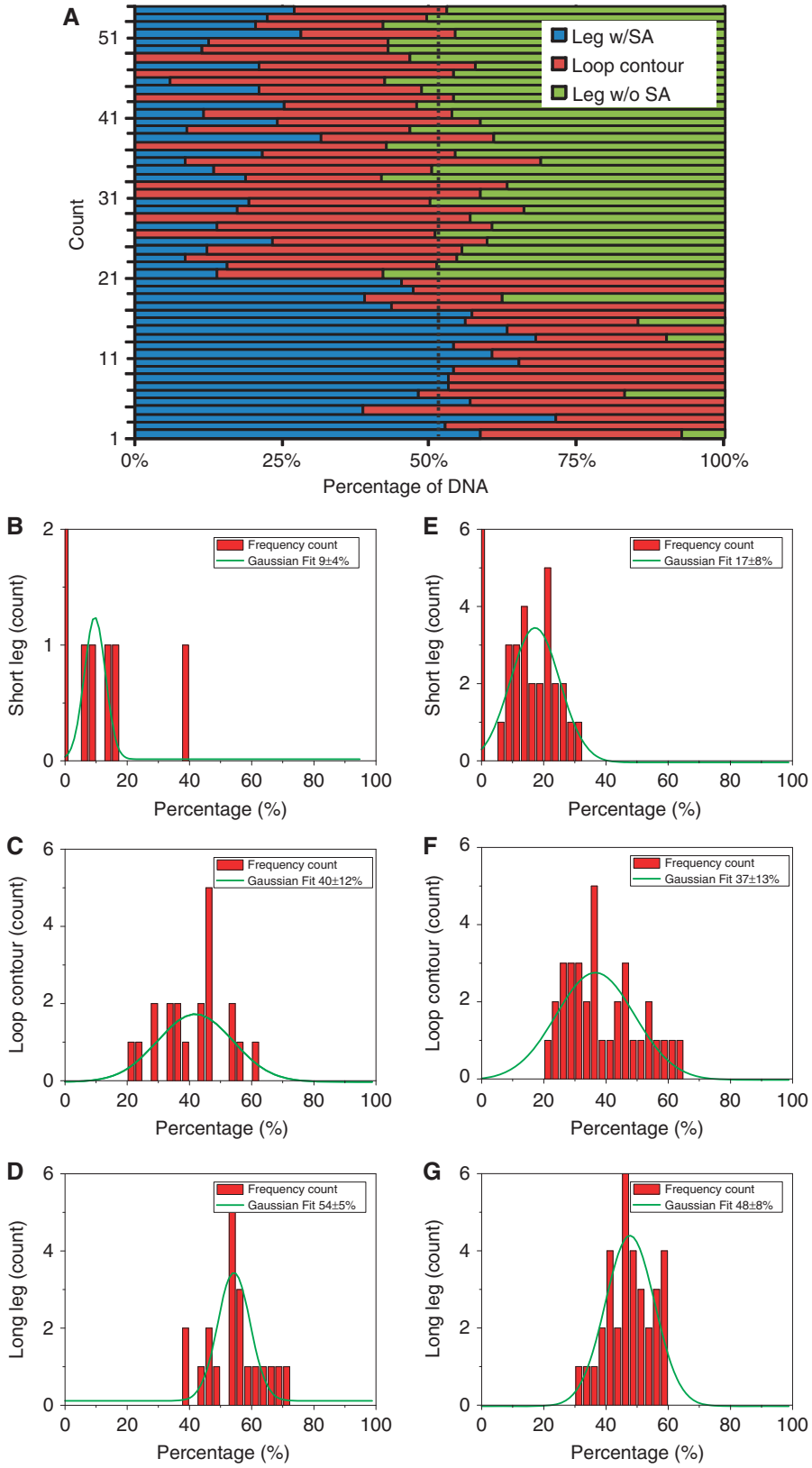

Figure 6 Normalized length distributions for MutS bound in loop configuration to heteroduplex DNA containing biotin at a single DNA end in the presence of ATP. MutS (100 nM) and 1120-bp G-T mismatch DNA (20 nM) that contained biotin at the end further from the mismatch site and that had been previously bound with monovalent streptavidin (see Materials and Methods) were incubated in 20 mM Tris–HCl (pH 7.5), 100 mM K^+ glutamate, 5 mM $MgCl_2$, and 0.4 mM DTT for 10 min at room temperature in the presence of ATP. Panel (**A**) shows the contour lengths of each segment on individual DNA molecules. The colours of these segments have the same means as Figure 5. Two sets of loops can be observed from panel (**A**). Set one: the loops are between MutS and biotinylated ends, and set two: the loops are between MutS and free ends. The histograms (**B–D**) and (**E–G**) show Gaussian fits of the contour length data of these two sets of loops, respectively.

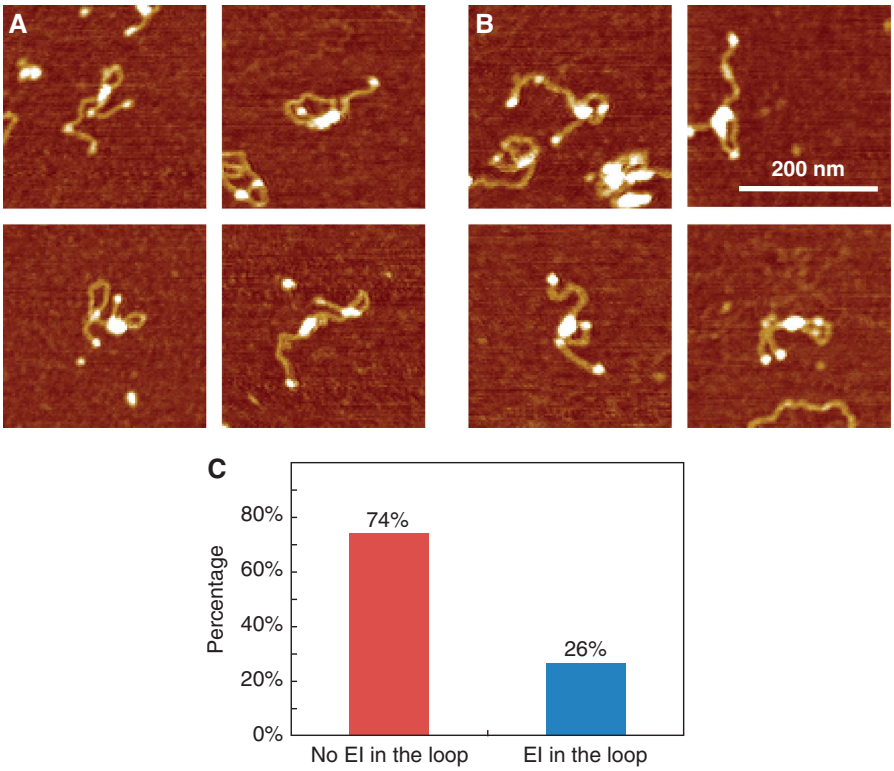

Figure 7 AFM images showing MutS/DNA loops with and without other proteins bound inside the loop. MutS (100 nM in Tris–K^+ glutamate buffer) was incubated with G-T heteroduplex DNA which had been previously bound with 50 nM streptavidin and 100 nM $EcoRI_{E111Q}$. ATP was added after MutS. Panel (**A**) shows loops without any $EcoRI_{E111Q}$ within the loop contour; panel (**B**) shows loops with *Eco*RI inside. The percentage histogram in panel (**C**) indicates the frequency of each type of loop.

may dissociate and rebind within 10 min incubation in our experiments. This effect would explain the observation that 26% of DNA loops contained $EcoRI_{E111Q}$ inside the loop contour (Figure 7). These observations support the idea that MutS moves along the DNA contour by means of a translocation (sliding) mechanism. In addition, our results strongly suggest that at least part of the enzyme, possibly one dimer of a tetramer, must remain at or near its target site (mismatch site). Moreover, DNA is being reeled from one side of the mismatch site, thereby producing expanding DNA loops. Adding ATP has the effect of making the size of the loop increase, and present observations support MutS translocation which depends on the binding of ATP. Looking ahead into the future, whether or not MutS translocation is ATP hydrolysis dependent needs to be clarified. Moreover, when AMPPnP was added (in Table II), the loop size can expand too. It might imply that ATP hydrolysis is not completely necessary for this unidirectional 'translocation'.

In conclusion, the AFM data presented here support the notion that MutS tetramers are involved in the early stages of MMR. MutS tetramers can be observed bound to heteroduplex DNA in a configuration in which one of the MutS dimers is closely associated with the mismatch site, while the other occupies a non-specific site. Both dimers are found at the base of DNA loops, the size of which increases in the presence of ATP. This growth is partially inhibited by protein roadblocks. Taken together, our results provide new insights into the mechanisms of MMR initiation in *E. coli* by MutS, and also reconcile the main features of sliding and looping models for the interaction of DNA mismatch and GATC sites.

Materials and methods

Proteins

MutS (Blackwell *et al*, 2001a) and $EcoRI_{E111Q}$ (Wright *et al*, 1989) were purified by published methods. Expression plasmids for 'live' (wt) and 'dead' (N23A/S45A/S27D) streptavidin were obtained from Alice Ting, Mass. Inst. of Technology. Monovalent streptavidin containing one active (biotin binding) subunit and three inactive subunits was prepared in accord to Howarth *et al* (2006).

DNA substrates

Linear 41- and 201-bp DNAs containing a G-T mismatch or an A/T base pair at a specific site were prepared as described previously (Blackwell *et al*, 2001a). Linear 1120-bp G-T mismatch and A-T homoduplex DNAs were prepared following the same protocol used by Pluciennik and Modrich (2007), except that 5′-TTACGCTTT CAGGTCAGAAGGGTTCTATTT-3′ and 5′-TTCATGCCGGAGAGGG TAGCTATTTTTG-3′ were used as primers, and phages f1MR65 and f1MR66 were used as templates. For both 1120-bp DNAs, two *Eco*RI binding sites are present, one 40% and one 81% of the DNA length from the end. In the 1120-bp G-T substrate, the G-T mismatch is located 53% of the distance from the same end (see Supplementary Figure S2A–C). PCRs were performed in which one or both primers were biotinylated at the 5′ ends, so that the final products contained biotin at one end (single-biotin DNAs) or both ends (double-biotin DNAs). Since the position of the mismatch on the DNA was known and a specific end of the DNA could be identified by streptavidin bound to single-biotin DNA, we were able to discriminate between MutS bound at a mismatch (specific complex) and MutS bound at a homoduplex site (non-specific complex) on single-biotin DNAs, by measuring the distance from MutS to the ends of the DNA. For both heteroduplex and homoduplex DNA, they were annealed using the same method.

Binding of $EcoRI_{E111Q}$ MutS, and streptavidin to 41-, 201-, and 1120-bp DNAs

MutS was diluted in dilution buffer daily for each experiment (20 mM KPO_4 pH 7.4, 150 mM KCl, 1 mM EDTA, and 1 mM DTT)

to a concentration of 0.5–2 μM monomer and kept on ice until use. DNA binding reactions (10 μl) contained 20 mM Tris–HCl pH 7.5, 100 mM K^+ glutamate, 5 mM $MgCl_2$, 0.4 mM DTT, 100 nM MutS, and 200 nM linear heteroduplex or homoduplex DNA (for 41- and 201-bp substrates) or 40–200 nM MutS and 5–20 nM DNA (for 1120-bp substrates). For comparison, in some experiments, HEPES reaction buffer (50 mM HEPES-KOH pH 8.0, 20 mM KCl, 5 mM $MgCl_2$, and 1 mM DTT) or phosphate reaction buffer (20 mM KPO_4 pH 7.4, 20 mM KCl, 5 mM $MgCl_2$, and 1 mM DTT) was used. Also, in some experiments, ATP, ADP, or AMPPnP was added to a final concentration of 0–2 mM. For $EcoRI_{E111Q}$ binding, 100 nM $EcoRI_{E111Q}$ (as dimer) was mixed with 10 nM 1120-bp DNA in Tris–K^+ glutamate reaction buffer in a total volume of 10 μl. The solution was incubated at room temperature for 10 min. The solution was then either used directly for AFM imaging, or components were added before AFM imaging was performed. For streptavidin which was previously bound, 50 nM streptavidin was mixed with 10 nM DNA (previously bound with 100 nM $EcoRI_{E111Q}$ or mock previously bound) and the solution was incubated at room temperature for 10 min. $EcoRI_{E111Q}$ and streptavidin binding were evaluated by AFM imaging. The statistical results show that about 61% of DNA had both ends blocked by $EcoRI_{E111Q}$. For double-biotin labelled DNA, 78% of DNA had both ends blocked by streptavidin. For single-biotin labelled DNA, 89% of DNA had one end blocked by streptavidin. These specific percentages are not critical, because when contour lengths or a K_D was determined, only the DNA molecules with both ends blocked by streptavidin were counted (for experiments with double-biotin labelled DNA). Control reactions were performed in the absence of $EcoRI_{E111Q}$ as well as the absence of streptavidin. For MutS binding to 1120-bp DNA, MutS was incubated with DNA previously bound with $EcoRI_{E111Q}$ and/or streptavidin in a total volume of 10 μl at room temperature for 10 min, followed by addition of nucleotide from 10 s to 10 min. Following incubation, the mixture was immediately deposited directly onto an APS-mica surface.

AFM sample preparation and imaging

1-(3-Aminopropyl)silatrane-functionalized mica (APS-mica) was used as a substrate for the binding of MutS and DNA molecules. APS-mica was prepared as described by Shlyakhtenko *et al* (2003). A 2–3 μl droplet of MutS/DNA solution was deposited on the APS-mica surface at room temperature for 1–3 s. The sample was immediately rinsed with deionized water and air-dried before imaging. Images were taken using a Nanoscope IIIa MultiMode Scanning Probe Microscope (Veeco Instruments Inc., Santa Barbara, CA) in tapping mode with an E scanner. RTESP probes (Veeco) were used for imaging in the air. The spring constant of AFM cantilevers was 20–80 N/m and their resonance frequency was 275–316 kHz. All images were collected at a scan rate of 2.0–3.0 Hz, a scan resolution of 512 × 512 pixels, and scan sizes of 1000–5000 nm. For each reaction, at least three mica samples were prepared, and for each sample on mica, at least 9–16 images from different locations were captured.

Calculation of MW of MutS by volume measurements from AFM images

Volume measurements were performed using WSXM (Horcas *et al*, 2007) SPM software (Nanotec Electronica S.L.). AFM images were first treated using the Roughness Analysis Function to determine the relative height of the mica surface. Using this function, the standard deviation of the height of the APS-mica surface was found to be slightly <0.1 nm. The 'Flooding' function of the software was used to calculate the volume of the proteins. As the name 'Flooding' indicates that this method is based on setting all of the image values above a given threshold selected by the user to a constant value (in this case, the height of the mica surface). The threshold chosen was 0.2 nm (two times of the standard deviation of the height of the mica surface) higher than the calculated mica surface; this resulted in flooding of $>95\%$ of the mica surface. The final image resembles a picture of a flooded body of land. Once the process is finished, WSXM calculates the flooded volume of the islands (means proteins), and a volume distribution histogram was obtained for further analysis. For each experimental condition, at least six images were measured to obtain an average value and the standard deviations. The volumes of a series of different proteins with known molecular weights were measured by this method, and a standard curve was constructed for use as reference (see Supplementary Figure S1).

Supplementary data

Supplementary data are available at *The EMBO Journal* Online (http://www.embojournal.org).

Acknowledgements

We are grateful to Paul Modrich and the members of his laboratory, particularly to Celia Baitinger, for providing all DNA substrates, MMR enzymes, and other proteins for this study. We would also like to thank Paul Modrich, Celia Baitinger, Anna Pluciennik, and other members of the Modrich laboratory for many discussions and helpful suggestions. This work was supported in part by NSF grant MCB-0450835 and NIH grant 1R21-GM071197 to PEM and by the start-up fund from Southeast University to YJ (2009-81 and KJ2010479).

Author contribution: YJ performed the experiments and data analysis. YJ and PEM designed the project and wrote the manuscript.

Conflict of interest

The authors declare that they have no conflict of interest.

References

Acharya S, Foster PL, Brooks P, Fishel R (2003) The coordinated functions of the E. coli MutS and MutL proteins in mismatch repair. *Mol Cell* **12:** 233–246

Allen DJ, Makhov A, Grilley M, Taylor J, Thresher R, Modrich P, Griffith JD (1997) MutS mediates heteroduplex loop formation by a translocation mechanism. *EMBO J* **16:** 4467–4476

Bjornson KP, Blackwell LJ, Sage H, Baitinger C, Allen D, Modrich P (2003) Assembly and molecular activities of the MutS tetramer. *J Biol Chem* **278:** 34667–34673

Bjornson KP, Modrich P (2003) Differential and simultaneous adenosine di- and triphosphate binding by MutS. *J Biol Chem* **278:** 18557–18562

Blackwell LJ, Bjornson KP, Allen DJ, Modrich P (2001a) Distinct MutS DNA-binding modes that are differentially modulated by ATP binding and hydrolysis. *J Biol Chem* **276:** 34339–34347

Blackwell LJ, Wang ST, Modrich P (2001b) DNA chain length dependence of formation and dynamics of hMutS alpha(.)hMutL alpha(.)heteroduplex complexes. *J Biol Chem* **276:** 33233–33240

Burdett V, Baitinger C, Viswanathan M, Lovett ST, Modrich P (2001) *In vivo* requirement for RecJ, ExoVII, ExoI, and ExoX in methyl-directed mismatch repair. *Proc Natl Acad Sci USA* **98:** 6765–6770

Calmann MA, Nowosielska A, Marinus MG (2005) Separation of mutation avoidance and antirecombination functions in an Escherichia coli mutS mutant. *Nucleic Acids Res* **33:** 1193–1200

Cooper DL, Lahue RS, Modrich P (1993) Methyl-directed mismatch repair is bidirectional. *J Biol Chem* **268:** 11823–11829

Crampton N, Roes S, Dryden DTF, Rao DN, Edwardson JM, Henderson RM (2007) DNA looping and translocation provide an optimal cleavage mechanism for the type III restriction enzymes. *EMBO J* **26:** 3815–3825

Feng G, Tsui HCT, Winkler ME (1996) Depletion of the cellular amounts of the MutS and MutH methyl-directed mismatch repair proteins in stationary-phase Escherichia coli K-12 cells. *J Bacteriol* **178:** 2388–2396

Gradia S, Subramanian D, Wilson T, Acharya S, Makhov A, Griffith J, Fishel R (1999) hMSH2-hMSH6 forms a hydrolysis-independent sliding clamp on mismatched DNA. *Mol Cell* **3:** 255–261

Hall MC, Wang H, Erie DA, Kunkel TA (2001) High affinity cooperative DNA binding by the yeast Mlh1-Pms1 heterodimer. *J Mol Biol* **312:** 637–647

Hansma HG, Kasuya K, Oroudjev E (2004) Atomic force microscopy imaging and pulling of nucleic acids. *Curr Opin Struct Biol* **14:** 380–385

Horcas I, Fernandez R, Gomez-Rodriguez JM, Colchero J, Gomez-Herrero J, Baro AM (2007) WSXM: a software for scanning probe microscopy and a tool for nanotechnology. *Rev Sci Instrum* **78:** 013705

Howarth M, Chinnapen DJF, Gerrow K, Dorrestein PC, Grandy MR, Kelleher NL, El-Husseini A, Ting AY (2006) A monovalent streptavidin with a single femtomolar biotin binding site. *Nat Methods* **3:** 267–273

Huang SYN, Crothers DM (2008) The role of nucleotide cofactor binding in cooperativity and specificity of MutS recognition. *J Mol Biol* **384:** 31–47

Iyer RR, Pluciennik A, Burdett V, Modrich PL (2006) DNA mismatch repair: functions and mechanisms. *Chem Rev* **106:** 302–323

Jia YX, Bi LJ, Li F, Chen YY, Zhang CG, Zhang XE (2008) alpha-Shaped DNA loops induced by MutS. *Biochem Biophys Res Commun* **372:** 618–622

Junop MS, Obmolova G, Rausch K, Hsieh P, Yang W (2001) Composite active site of an ABC ATPase: MutS uses ATP to verify mismatch recognition and authorize DNA repair. *Mol Cell* **7:** 1–12

Kunkel TA, Erie DA (2005) DNA mismatch repair. *Annu Rev Biochem* **74:** 681–710

Lahue RS, Au KG, Modrich P (1989) DNA mismatch correction in a defined system. *Science* **245:** 160–164

Lamers MH, Georgijevic D, Lebbink JH, Winterwerp HH, Agianian B, de Wind N, Sixma TK (2004) ATP increases the affinity between MutS ATPase domains. Implications for ATP hydrolysis and conformational changes. *J Biol Chem* **279:** 43879–43885

Manelyte L, Urbanke C, Giron-Monzon L, Friedhoff P (2006) Structural and functional analysis of the MutS C-terminal tetramerization domain. *Nucleic Acids Res* **34:** 5270–5279

Mendillo ML, Putnam CD, Kolodner RD (2007) Escherichia coli MutS tetramerization domain structure reveals that stable dimers but not tetramers are essential for DNA mismatch repair *in vivo*. *J Biol Chem* **282:** 16345–16354

Mikheikin AL, Lushnikov AY, Lyubchenko YL (2006) Effect of DNA supercoiling on the geometry of Holliday junctions. *Biochemistry* **45:** 12998–13006

Modrich P (1987) DNA mismatch correction. *Annu Rev Biochem* **56:** 435–466

Modrich P, Lahue R (1996) Mismatch repair in replication fidelity, genetic recombination, and cancer biology. *Annu Rev Biochem* **65:** 101–133

Natrajan G, Lamers MH, Enzlin JH, Winterwerp HH, Perrakis A, Sixma TK (2003) Structures of Escherichia coli DNA mismatch repair enzyme MutS in complex with different mismatches: a common recognition mode for diverse substrates. *Nucleic Acids Res* **31:** 4814–4821

Obmolova G, Ban C, Hsieh P, Yang W (2000) Crystal structures of mismatch repair protein MutS and its complex with a substrate DNA. *Nature* **407:** 703–710

Pluciennik A, Modrich P (2007) Protein roadblocks and helix discontinuities are barriers to the initiation of mismatch repair. *Proc Natl Acad Sci USA* **104:** 12709–12713

Pukkila PJ, Peterson J, Herman G, Modrich P, Meselson M (1983) Effects of high levels of DNA adenine methylation on methyl-directed mismatch repair in *Escherichia coli*. *Genetics* **104:** 571–582

Ratcliff GC, Erie DA (2001) A novel single-molecule study to determine protein-protein association constants. *J Am Chem Soc* **123:** 5632–5635

Schofield MJ, Nayak S, Scott TH, Du CW, Hsieh P (2001) Interaction of Escherichia coli MutS and MutL at a DNA mismatch. *J Biol Chem* **276:** 28291–28299

Shlyakhtenko LS, Gall AA, Filonov A, Cerovac Z, Lushnikov A, Lyubchenko YL (2003) Silatrane-based surface chemistry for immobilization of DNA, protein-DNA complexes and other biological materials. *Ultramicroscopy* **97:** 279–287

Shlyakhtenko LS, Gilmore J, Portillo A, Tamulaitis G, Siksnys V, Lyubchenko YL (2007) Direct visualization of the EcoRII-DNA triple synaptic complex by atomic force microscopy. *Biochemistry* **46:** 11128–11136

Tessmer I, Yang Y, Zhai J, Du CW, Hsieh P, Hingorani MM, Erie DA (2008) Mechanism of MutS searching for DNA mismatches and signaling repair. *J Biol Chem* **283:** 36646–36654

Viswanathan M, Burdett V, Baitinger C, Modrich P, Lovett ST (2001) Redundant exonuclease involvement in *Escherichia coli* methyl-directed mismatch repair. *J Biol Chem* **276:** 31053–31058

Wang H, Yang Y, Schofield MJ, Du CW, Fridman Y, Lee SD, Larson ED, Drummond JT, Alani E, Hsieh P, Erie DA (2003) DNA bending and unbending by MutS govern mismatch recognition and specificity. *Proc Natl Acad Sci USA* **100:** 14822–14827

Wang HX, Hays JB (2004) Signaling from DNA mispairs to mismatch-repair excision sites despite intervening blockades. *EMBO J* **23:** 2126–2133

Wright DJ, King K, Modrich P (1989) The negative charge of Glu-111 is required to activate the cleavage center of EcoRI endonuclease. *J Biol Chem* **264:** 11816–11821

Yang Y, Sass LE, Du CW, Hsieh P, Erie DA (2005) Determination of protein-DNA binding constants and specificities from statistical analyses of single molecules: MutS-DNA interactions. *Nucleic Acids Res* **33:** 4322–4334